Bratislava Medical Journal
https://doi.org/10.1007/s44411-026-00534-0

RESEARCH

The Effect of Hyperbaric Oxygen Therapy on Autophagic and Apoptotic Changes in the Hippocampal Region Resulting from Folic Acid Deficiency Induced by Methotrexate in Male Rat Brains

A. Cabir[1] · M. A. Baktır[2] · B. F. Kıryar[3] · M. Ermiş[4] · E. Çolak[1] · F. Beyaz[1,3]

Received: 9 December 2025 / Revised: 14 January 2026 / Accepted: 5 February 2026
© The Author(s) 2026

Abstract

Background Methotrexate (MTX), a widely used antifolate agent in oncology and autoimmune disorders, has been increasingly associated with neurotoxic effects in the central nervous system. Hyperbaric oxygen (HBO) therapy has emerged as a potential neuroprotective approach through modulation of oxidative stress and cellular stress-response pathways, including autophagy and apoptosis. However, the region-specific effects of MTX and HBO on the autophagy–apoptosis axis within the hippocampus remain incompletely understood.

Materials and Methods Adult male Sprague Dawley rats were randomly assigned to four groups: SALINE, HBO, MTX, and MTX + HBO. Hippocampal dentate gyrus (DG) and cornu ammonis (CA) subregions were analyzed. Immunohistochemistry was used to assess autophagy- and apoptosis-related markers, including LC3, Beclin-1, p62/SQSTM1, and cleaved Caspase-3 (Asp175). DNA fragmentation was evaluated using the TUNEL assay. Quantitative analyses were performed using animal-based mean values, and statistical comparisons were conducted using one-way ANOVA followed by Tukey post hoc testing ($p < 0.05$).

Results MTX administration was associated with increased LC3 and Beclin-1 immunoreactivity, indicating activation of early-phase autophagy-related signaling, accompanied by p62 accumulation and elevated Caspase-3 immunoreactivity, a pattern consistent with disrupted downstream autophagic processing and enhanced apoptotic signaling. HBO treatment alone induced a more limited increase in LC3 and Beclin-1 while reducing basal p62 and Caspase-3 levels, suggesting a modulatory and adaptive cellular response rather than overt stress activation. In the MTX + HBO group, p62 and Caspase-3 levels were reduced relative to MTX alone, indicating partial attenuation of MTX-associated cellular stress. TUNEL labeling was negative in all groups, suggesting that apoptotic processes were captured at an early or pre-fragmentation stage.

Conclusions The present findings indicate that MTX exposure is associated with preserved autophagy initiation signals but impaired downstream processing and increased apoptotic signaling in the hippocampus. HBO treatment appears to modulate this imbalance by attenuating autophagy-associated stress and apoptotic signaling in a region-dependent manner, without providing definitive evidence of fully restored autophagic flux. These results support the biological plausibility of HBO as an adjunctive strategy to mitigate MTX-associated hippocampal stress while underscoring the need for future studies incorporating direct flux assessments, sex-specific analyses, and functional outcomes.

Keywords Methotrexate · Hyperbaric oxygen · Hippocampus · Autophagy · Neurotoxicity

1 Introduction

Methotrexate (MTX), a folate antagonist first introduced in clinical practice after the synthesis of aminopterin in the mid-twentieth century [1], remains a cornerstone in the treatment of malignancies and autoimmune disorders [2, 3]. At high doses, MTX is used as chemotherapy for hematological cancers and osteosarcoma, whereas at lower doses it is prescribed for chronic inflammatory conditions such as rheumatoid arthritis, psoriasis, lupus, and inflammatory bowel disease [4]. Its mechanism of action involves inhibition of dihydrofolate reductase (DHFR), thereby interfering with nucleotide synthesis and impairing DNA, RNA, and protein production, particularly in rapidly dividing cells [5]. In addition, MTX exerts immunomodulatory effects by promoting

Extended author information available on the last page of the article

extracellular adenosine accumulation and modulating cytokine release [3].

Despite its therapeutic benefits, MTX is associated with toxicity in several organs, including the liver, kidneys, testes, and central nervous system. Neurotoxic effects of MTX are thought to result from oxidative stress, mitochondrial dysfunction, lipid peroxidation, and disruption of antioxidant defenses [5, 6]. Moreover, MTX has been shown to alter autophagy and apoptosis signaling. Reports indicate increased expression of Beclin-1 and LC3, impaired autophagic flux reflected by p62 accumulation, and a shift in the Bax/Bcl-2 ratio leading to apoptosis [6].

Hyperbaric oxygen therapy (HBO) is a well-established treatment modality that involves the administration of 100% oxygen at pressures exceeding atmospheric levels, usually between 1.4 and 3 atmospheres absolute (ATA). Under such conditions, the partial pressure of oxygen in plasma and tissues increases substantially, leading to enhanced oxygen delivery to hypoxic areas [7]. According to the Undersea and Hyperbaric Medical Society (UHMS), HBO is clinically indicated in disorders such as carbon monoxide poisoning, decompression sickness, chronic wounds, radiation necrosis, and diabetic ulcers [8, 9]. Beyond these approved uses, experimental studies have revealed that HBO exerts pleiotropic biological effects, including the reduction of oxidative stress, stabilization of mitochondrial activity, suppression of inflammatory cascades, and enhancement of tissue repair and angiogenesis [10–13].

Recent evidence suggests that HBO also regulates intracellular quality control pathways such as autophagy, a conserved catabolic process essential for maintaining cellular homeostasis. Autophagy involves the sequestration of cytoplasmic components into autophagosomes and their subsequent degradation via lysosomes, a mechanism crucial for eliminating damaged organelles and misfolded proteins [14, 15]. Several studies have reported that HBO modulates autophagy-related proteins, such as microtubule-associated protein 1 light chain 3 (LC3) and Beclin-1, and influences p62/SQSTM1 turnover, thereby impacting neuronal survival under stress conditions. By fine-tuning autophagy, HBO may serve as a protective mechanism against both hypoxia-induced and drug-induced cytotoxicity [15].

The hippocampus is highly susceptible to oxidative and metabolic stress, making it a critical site for studying the combined effects of MTX and HBO. This brain region is essential for learning, memory, and emotional regulationand is composed of distinct subfields with heterogeneous structural and functional properties. The CA1 region is particularly sensitive to ischemia and excitotoxicity [16]. The CA2 subfield, though smaller and less studied, has unique synaptic connectivity and plays a role in social memory [17]. The CA3 region, characterized by recurrent collaterals, is vulnerable to oxidative and excitotoxic insults and is central to pattern completion in memory [18]. The CA4 region, embedded within the hilus of the dentate gyrus, contributes to hippocampal excitability and neurogenesis [19, 20]. The dentate gyrus (DG) is a site of adult neurogenesis and is involved in pattern separation, where autophagy is critical for neuronal survival and synaptic plasticity [21]. Additionally, as a conspicuous part of the limbic system, the hippocampus is key to learning and memory processes, as well as the regulation of emotional and sexual behavior [22, 23].

Growing evidence indicates that autophagy and apoptosis in these hippocampal subfields are dynamically regulated under pathological conditions. For instance, experimental studies have shown region-specific vulnerability of CA1versus CA3 neurons to oxidative stress and mitochondrial damage [24]. Moreover, alterations in autophagy-related proteins such as LC3, Beclin-1, and p62 have been associated with impaired synaptic plasticity and neuronal loss in hippocampal subregions. Apoptotic markers, including Caspase-3, are also frequently elevated under neurotoxic conditions, further contributing to hippocampal dysfunction [25, 26].

In this context, the present study was designed to investigate the effects of low-dose MTX and HBO on hippocampal autophagy and apoptosis, focusing specifically on the CA1, CA2, CA3, CA4, and DG subfields. By evaluating immunohistochemical expression of LC3, Beclin-1, and p62 as autophagy-related markers, alongside Caspase-3 as an apoptotic indicator, we aimed to clarify the cellular mechanisms through which HBO modulates MTX-induced alterations in hippocampal homeostasis.

2 Materials and Methods

2.1 Design of Experiments and Ethical Approval

This study was approved (22/120) by the Local Ethics Committee for Animal Experiments of Erciyes University and conducted in strict accordance with international guidelines for the ethical care and use of laboratory animals. A total of 28 male Sprague Dawley (SD) rats (220–250 g) were obtained from the Experimental Research and Application Center (DEKAM), Erciyes University. The animals were housed under standardized laboratory conditions (22 ± 2 °C; 12-h light/dark cycle) at the Experimental Research Center of Erciyes University, with free access to standard chow and water. All procedures involving animal handling and maintenance were performed under controlled conditions to ensure animal welfare throughout the experimental period.

2.2 Experimental Procedures

Animal experiments were carried out during the period from September 2022 to October 2022. Hyperbaric oxygen treatment (2 ATA, 1 h/day) was administered based on the standardized protocol previously validated in the study of Baktır et al. (2024) [27]. Animals were divided into four groups. In the saline group (Saline, n = 7), the animals received intraperitoneal injections of normal saline (0.9% NaCl) on days 8 and 15 of the experiment. In the methotrexate group (MTX, n = 7), the animals received intraperitoneal injections of liquid methotrexate (25 mg/kg) on days 8 and 15 corresponding to two systemic MTX administrations over a 15-day experimental period. In the methotrexate plus hyperbaric oxygen group (MTX + HB, n = 7), the animals received intraperitoneal injections of liquid methotrexate (25 mg/kg) on days 8 and 15, followed by hyperbaric oxygen therapy at 2 atmospheres for 1 h daily for 15 consecutive days. In the hyperbaric oxygen group (HB, n = 7), the animals received hyperbaric oxygen therapy at 2 atmospheres for 1 h daily for 30 consecutive days.

2.3 Tissue Harvesting Procedures

At the end of the experimental period, general anesthesia was induced in all rats in accordance with the approved protocol. A combination of ketamine (60 mg/kg) and xylazine (10 mg/kg) was administered intraperitoneally using a 1 cc insulin syringe. This anesthetic regimen has been widely employed in rats as it provides reliable sedation, sufficient analgesia, and muscle relaxation, together with rapid induction and stable maintenance of anesthesia [28]. The adequacy of anesthesia was confirmed by the absence of pedal reflex and by monitoring respiratory patterns. Following anesthesia, the brains of all animals were excised after transcardiac perfusion. Initially, physiological saline (0.9% NaCl) was perfused to flush the vascular system, after which Bouin's fixative solution was introduced intravascularly to preserve tissue morphology and ensure optimal fixation. Subsequently, the brains were removed and immersed in Bouin's solution for 14 h for post-fixation. For histological and immunohistochemical processing, the fixed tissues were passed through a graded ethanol series (50%, 70%, 80%, 96%, and absolute ethanol) for dehydration. The samples were then cleared in methyl benzoate and benzene before being embedded in paraffin blocks. Serial sections of appropriate thickness were prepared from the paraffin-embedded tissues and reserved for subsequent histological and immunohistochemical analyses [29].

2.4 Immunohistochemistry

Strept(avidin)–Biotin method immunohistochemistry was performed to evaluate the expression of LC3, Beclin-1, p62, and Cleaved Caspase-3 (Asp175) in brain tissues. Detailed information regarding the primary antibodies used is provided in Table 1. Tissue sections were initially deparaffinized in xylene and rehydrated through a graded ethanol series, followed by rinsing in distilled water. Antigen retrieval was conducted using a citrate buffer solution (pH 6.0), with the sections heated to 95 °C for 15 min to unmask the antigenic epitopes. After cooling to room temperature, the sections were rinsed thoroughly with phosphate-buffered saline (PBS). To minimize nonspecific background staining, endogenous peroxidase activity was blocked by incubating the sections in hydrogen peroxide solution for 15 min. Antigen retrieval was then performed by immersing the sections in citrate buffer (pH 6.0) and heating at 95 °C for 15 min**.** Protein blocking was then performed using Ultra V Block (Thermo Scientific) for 10 min at room temperature. After blocking, the sections were incubated overnight at 4 °C in a humidified chamber with the following primary antibodies: LC3 (1:400), Beclin-1 (1:200), p62 (1:200), and Cleaved Caspase-3 (Asp175) (1:10), detailed information regarding dilution ratios, host species, clonality, and manufacturers of these antibodies is provided in Table 1**.** On the following day, excess unbound primary antibodies were removed by washing with PBS. Biotinylated secondary antibodies (anti-mouse and anti-rabbit; Thermo Scientific) were applied to the sections for 10 min at room temperature. Subsequently, horseradish peroxidase (HRP)-conjugated streptavidin (Thermo Scientific) was added to amplify the signal for 10 min at room temperature. Immunoreactivity was visualized using 3,3′-diaminobenzidine (DAB), producing a brown precipitate at the site of antigen–antibody binding. Finally, cellular morphology was enhanced by

Table 1 Detailed information regarding the primary antibodies used in this study, including company, catalog number, host species, clonality, dilution factor, and species reactivity

Antibody	Company	Cat No	Host, clonality	Dilution	Species reactivity
LC3αβ	Santa Cruz	Sc-398822	Mouse monoclonal	1:400	Human, mouse, rat
Beclin1	Santa Cruz	Sc-48341	Mouse, monoclonal	1:200	Human, mouse, rat,
SQSTM1/p62	Santa Cruz	Sc-48402	Mouse, monoclonal	1:200	Human, mouse, rat,
Cleaved Caspase-3	Merck Millipore	AB3623	Rabbit, polyclonal	1:10	Human, mouse, rat

counterstaining the sections with Gill's hematoxylin, which provided a clear blue nuclear contrast [30].

To validate the specificity of immunohistochemical staining, positive and negative controls were included (Fig. 1). For positive controls, tissues known to express the respective proteins were used: LC3 (testis), Beclin-1 (cardiac muscle), p62/SQSTM1 (lung), and Caspase-3 (kidney). Negative controls were prepared by omitting the primary antibody in hippocampal sections, which showed no immunoreactivity. Figure 2. Positive and negative immunohistochemical controls used in the study. (a) LC3 immunoreactivity in testis (positive control). (b) Beclin-1 immunoreactivity in cardiac muscle (positive control). (c) p62/SQSTM1 immunoreactivity in lung tissue (positive control). (d) Caspase-3 immunoreactivity in kidney tissue (positive control). (e) LC3 negative control in hippocampal section (primary antibody omitted). (f) Beclin-1 negative control in hippocampal section (primary antibody omitted). (g) p62/SQSTM1 negative control in hippocampal section (primary antibody omitted). (h) Caspase-3 negative control in hippocampal section (primary antibody omitted). Scale bars: 20 µm (a–d); 50 µm (e–h).

2.5 Imaging and Photographing

For histological and immunohistochemical examinations, hippocampal sections were analyzed using an Olympus BX51 light microscope, which provides high-resolution imaging. Digital recordings were obtained with an integrated Olympus DP71 camera system, and all images were captured under standardized conditions at × 20 magnification. During imaging, distinct morphological regions of the hippocampus, including CA1, CA2, CA3, CA4, and DG, were separately focused and photographed, ensuring representative documentation of each subfield.

2.6 Statistical analyses

The acquired images were subsequently analyzed using Fiji software (ImageJ-based, latest version). Initially, all images were renamed and standardized in resolution, followed by calibration to enable measurements at the micrometer level. For immunohistochemical evaluation, color deconvolution and grayscale conversion were performed to enhance the visibility of positive signals. Subsequently, thresholding techniques were applied to distinguish specific staining from background. Quantitative parameters, including the percentage of positive staining and the total measured area, were extracted.

The statistical analyses of the obtained data were performed using GraphPad Prism software (version 10.6.0). Normality of the data distribution was assessed, followed by the application of appropriate parametric or non-parametric statistical tests. Results were expressed as mean ± SD, and a value of $p < 0.05$ was considered statistically significant.

2.7 Findings

2.7.1 LC3 Expression in the CA1 Region

Immunohistochemical staining with the LC3 antibody revealed clear variations among the experimental groups in the CA1 hippocampal subfield (Fig. 3a–d). Positively stained cells are shown with black arrows. The MTX group exhibited the greatest proportion of LC3-positive staining ($p < 0.05$), indicating that methotrexate markedly stimulates autophagy in this region. This was followed in descending order by the MTX + HBO group, the HBO group, and finally the SALINE group, which displayed the lowest expression. Importantly, LC3 immunoreactivity in the MTX + HBO group was noticeably lower than that observed in MTX alone, suggesting that HBO treatment alleviates the excessive autophagy triggered by MTX. Statistical evaluation was carried out using one-way ANOVA, with post-hoc comparisons performed by the Tukey test. Groups labeled with different letters were considered significantly different ($p < 0.05$).

2.7.2 LC3 Expression in the CA2 Region

A comparable staining distribution was detected in the CA2 region (Fig. 3f–i), where positive cells are indicated by black arrow. The MTX group again showed the highest percentage of LC3-positive area ($p < 0.05$). This was followed by the MTX + HBO group, then the HBO group, and lastly the SALINE group. Expression in the MTX + HBO group was lower than MTX alone but remained higher than in SALINE and HBO animals, implying that HBO co-administration can partly counterbalance MTX-induced changes.

Interestingly, the HBO group presented a moderate increase relative to SALINE, suggesting that HBO on its own may exert a mild stimulatory effect on autophagy. Statistical analysis using one-way ANOVA with Tukey's post-hoc test confirmed significant group differences ($p < 0.05$).

2.7.3 LC3 Expression in the CA3 Region

In the CA3 region, LC3 expression also differed significantly across the groups (Fig. 3k–n). Positive staining was visualized with black arrow. The MTX group demonstrated the highest level of LC3 immunoreactivity ($p < 0.05$), followed by the MTX + HBO group, the HBO group, and the SALINE group. The reduced levels in MTX + HBO compared to MTX alone emphasize the protective effect of HBO in

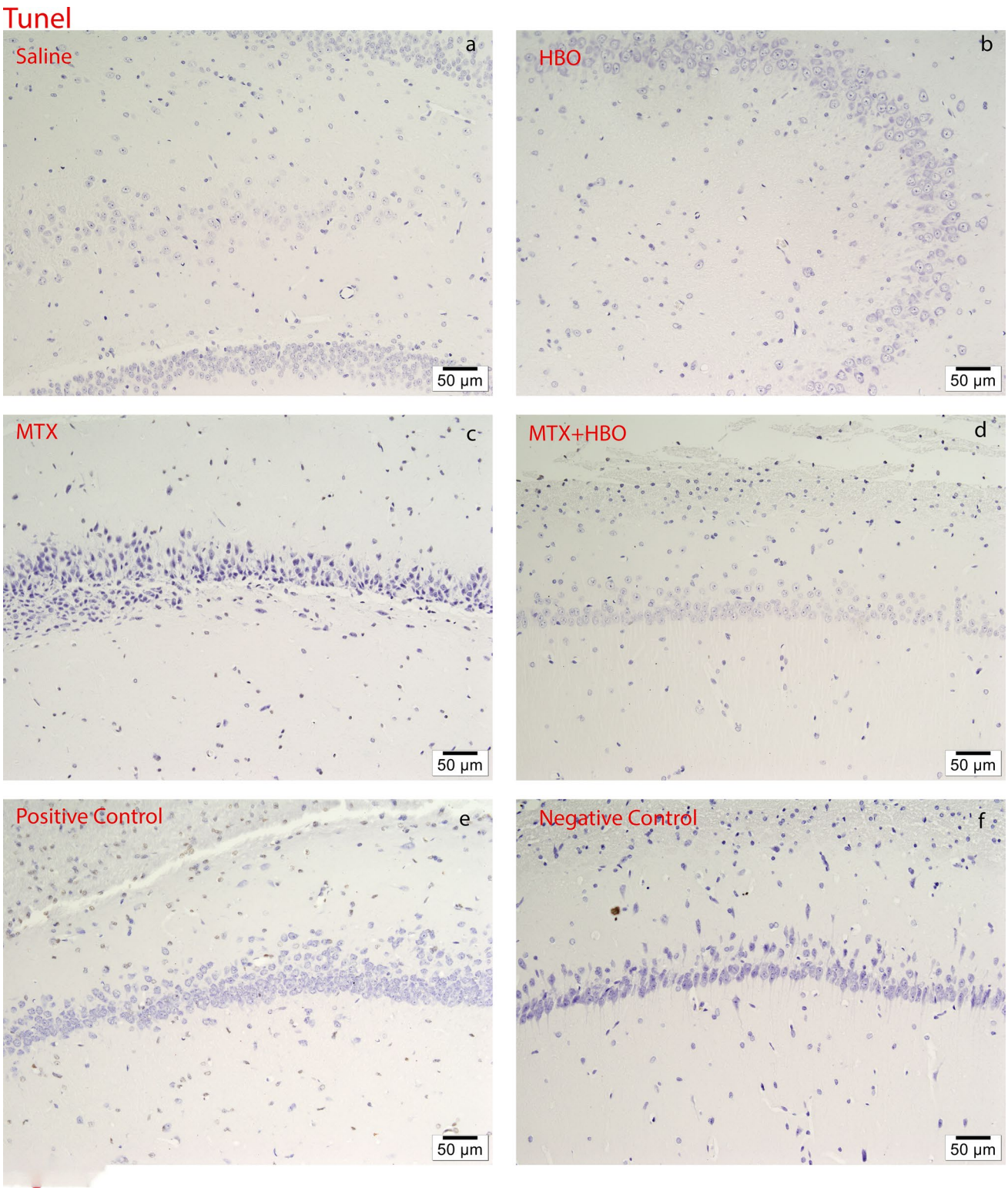

Fig. 1 Representative TUNEL staining in hippocampal sections from the experimental groups: SALINE (**a**), HBO (**b**), MTX (**c**), and MTX + HBO (**d**). Positive control (**e**) and negative control (**f**) sections are also shown. No TUNEL-positive nuclei were detected in any experimental groups. Scale bars = 50 µm

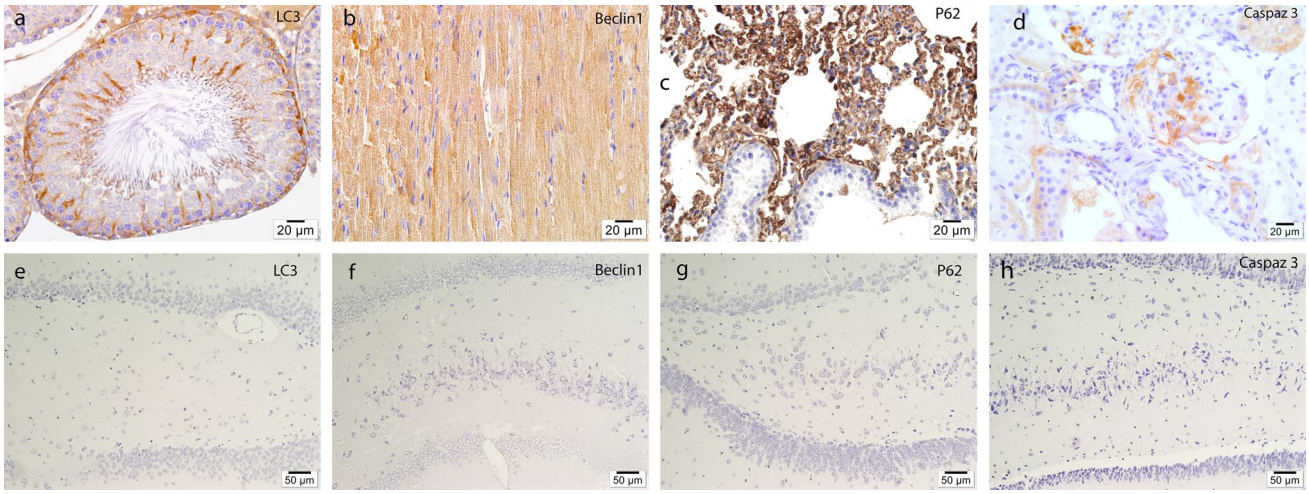

Fig. 2 Representative immunohistochemical staining for LC3 (**a**, **e**), Beclin-1 (**b**, **f**), p62 (**c**, **g**), and Caspase-3 (**d**, **h**). Positive control tissues: testis (**a**), cardiac muscle (**b**), lung (**c**), and kidney (**d**) sections show specific immunoreactivity (scale bars = 20 µm). Corresponding negative control hippocampal sections (**e**–**h**) display the absence of staining (scale bars = 50 µm)

limiting MTX-driven autophagy. The SALINE group consistently displayed the lowest baseline values.

Data analysis with ANOVA and Tukey's test verified that the intergroup differences were statistically significant ($p < 0.05$).

2.7.4 LC3 Expression in DG & CA4 Regions

In the DG and CA4 regions, LC3 immunoreactivity displayed a consistent distribution pattern (Fig. 3p–t). Positively stained cells are highlighted with black arrow. The MTX group again exhibited the greatest proportion of LC3-positive area ($p < 0.05$), followed in order by the MTX + HBO group, the HBO group, and finally the SALINE group. Expression levels in the MTX + HBO group were markedly lower than MTX alone but remained higher than SALINE, supporting the notion that HBO co-treatment alleviates MTX-induced autophagic activity. For statistical evaluation, a one-way ANOVA followed by the Tukey post-hoc test was applied. Groups marked with distinct letters above the bars in the graphs were regarded as significantly different at the $p < 0.05$ level.

2.7.5 Cleaved Caspase-3 (Asp175) Expression Findings

2.7.5.1 CA1 Region Immunohistochemical staining for Caspase-3 in the CA1 region revealed significant differences among the groups (Fig. 4a–d, e). Positively stained apoptotic cells are marked with black arrows. The MTX group exhibited the highest Caspase-3 expression ($p < 0.05$), consistent with methotrexate-induced apoptosis. This was followed by the HBO group and the MTX + HBO group, while the SALINE group displayed the lowest expression. Interestingly, Caspase-3 expression in the MTX + HBO group was significantly lower compared to MTX alone, suggesting that HBO treatment mitigates MTX-induced apoptosis.

2.7.5.2 CA2 Region In the CA2 region, a similar pattern of Caspase-3 expression was observed (Fig. 4f–i, j). Positive cells are indicated with black arrows. The MTX group again showed the strongest staining ($p < 0.05$), followed by HBO, MTX + HBO, and SALINE. The significant reduction in Caspase-3 expression in the MTX + HBO group compared with MTX highlights the anti-apoptotic influence of HBO. The SALINE group consistently displayed minimal expression, indicating baseline apoptotic activity.

2.7.5.3 CA3 Region Caspase-3 immunoreactivity in the CA3 region of the hippocampus also demonstrated distinct intergroup differences (Fig. 4k–n, o). Black arrows mark positive apoptotic cells. The MTX group exhibited the highest expression ($p < 0.05$), whereas the HBO group showed moderate expression. The MTX + HBO group presented a marked decrease compared to MTX, while the SALINE group had the lowest levels. These results confirm that MTX strongly promotes apoptosis in CA3 neurons, while HBO exerts a protective effect when combined with MTX.

2.7.5.4 DG & CA4 Regions In the DG and CA4 regions, numerous Caspase-3 immunopositive cells were detected in the MTX group, as highlighted by black arrows (Fig. 4p–t, u). Quantitative assessment revealed that the MTX group had the greatest Caspase-3 expression ($p < 0.05$), followed by HBO, MTX + HBO, and SALINE groups. Expression levels in the MTX + HBO group were mark-

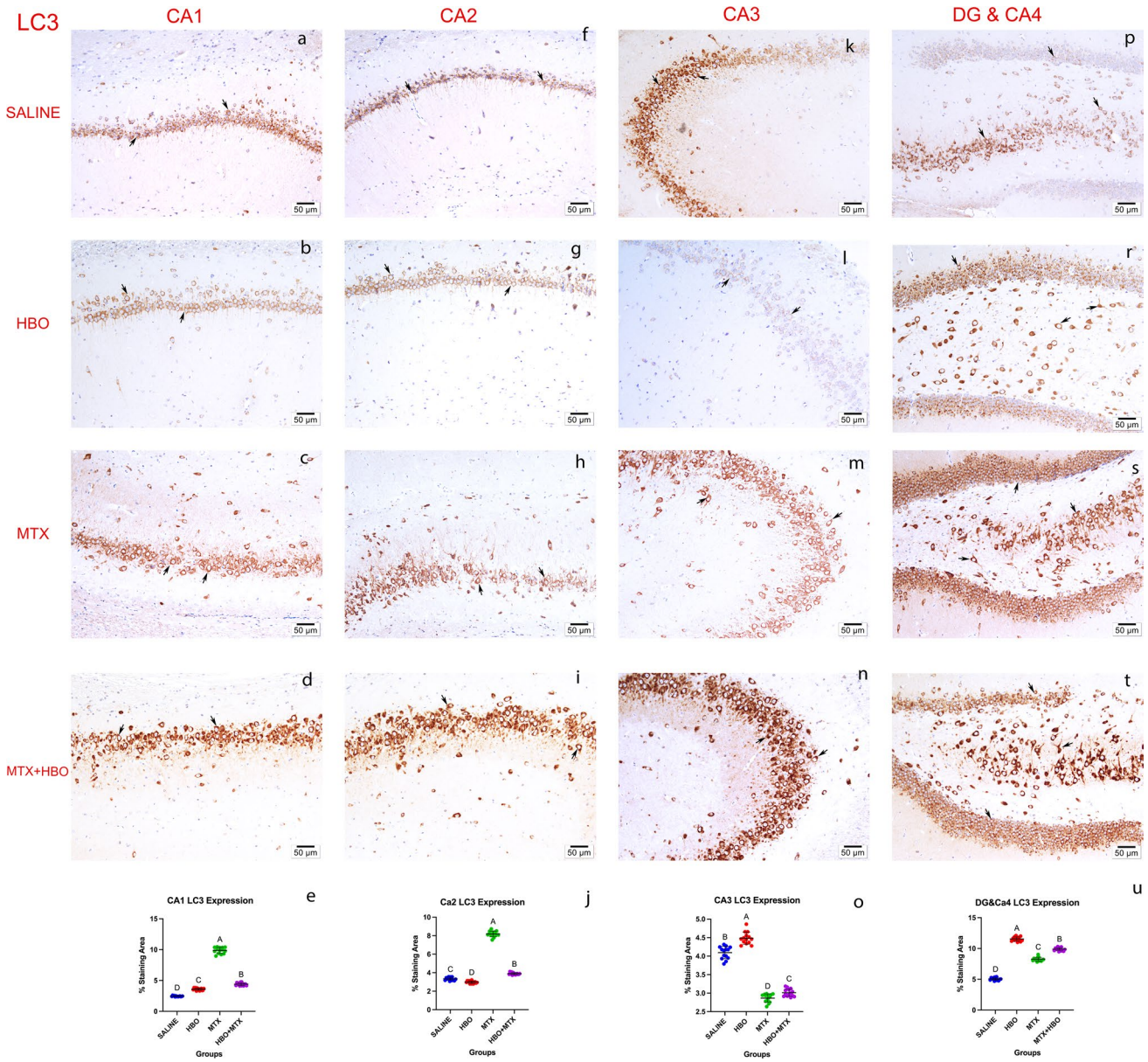

Fig. 3 Representative immunoreactivity showing LC3 immunoreactivity in hippocampal subregions (CA1, CA2, CA3, DG&CA4) across experimental groups: SALINE (**a**, **f**, **k**, **p**), HBO (**b**, **g**, **l**, **r**), MTX (**c**, **h**, **m**, **s**), and MTX + HBO (**d**, **i**, **n**, **t**). Black arrow indicate LC3-positive cells. Panels (**e**, **j**, **o**, **u**) represent quantitative analyses of LC3 immunoreactivity expressed as % relative area in each subregion. Data are presented as dot plots showing individual animal values with mean ± SD. Serial sections were obtained from each animal, and two series were randomly selected per animal, with each series consisting of 12 sections. Quantification was performed using animal-based mean values, with each dot representing one animal (n = 7 per group). Different superscript letters indicate statistically significant differences between groups ($p < 0.05$). Scale bars = 50 µm

edly reduced compared with MTX alone, emphasizing the apoptosis-modulating and protective role of HBO therapy. Animals in the SALINE group consistently displayed the lowest Caspase-3 activity, reflecting baseline physiological apoptotic levels.

2.8 p62 Expression Findings

2.8.1 CA1 Region

Immunohistochemical staining for p62 in the CA1 region demonstrated significant differences among the groups (Fig. 5a–d, e). Positively stained cells are indicated

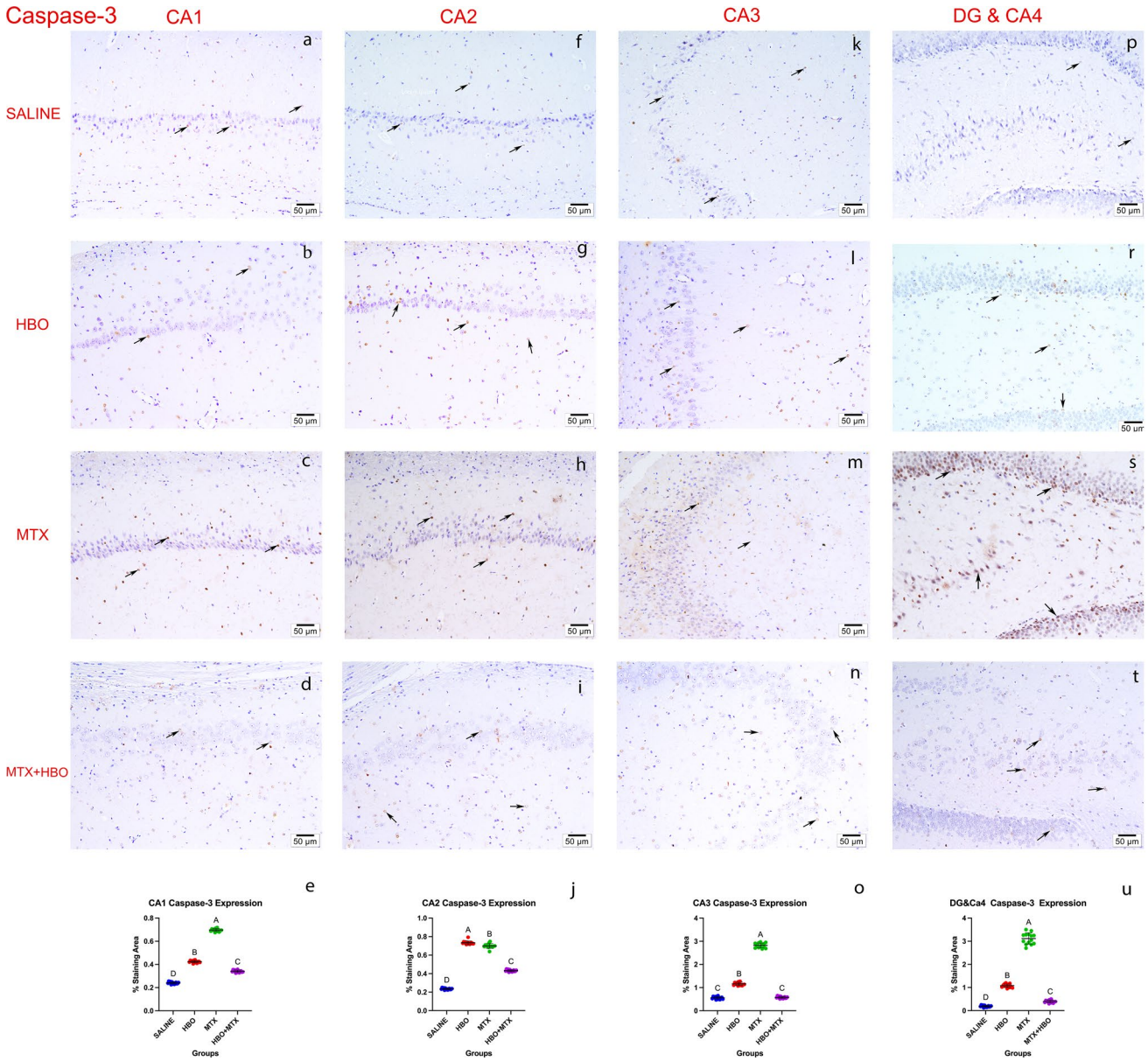

Fig. 4 Representative immunoreactivity images showing Cleaved Caspase-3 (Asp175) expression in hippocampal subregions (CA1, CA2, CA3, DG&CA4) across experimental groups: SALINE (**a**, **f**, **k**, **p**), HBO (**b**, **g**, **l**, **r**), MTX (**c**, **h**, **m**, **s**), and MTX + HBO (**d**, **i**, **n**, **t**). Black arrows indicate Caspase-3-positive cells. Panels (**e**, **j**, **o**, **u**) represent quantitative analyses of Caspase-3 immunoreactivity expressed as % relative area in each subregion. Data are presented as dot plots showing individual animal values with mean ± SD. Serial sections were obtained from each animal, and two series were randomly selected per animal, with each series consisting of 12 sections. Quantification was performed using animal-based mean values, with each dot representing one animal (n = 7 per group). Different superscript letters indicate statistically significant differences between groups ($p < 0.05$). Scale bars = 50 µm

with black arrow. The MTX group exhibited the highest p62 expression ($p < 0.05$), indicating increased autophagic flux impairment under methotrexate exposure. This was followed by the HBO group and the MTX + HBO group, whereas the SALINE groupshowed the lowest expression. Of note, the MTX + HBO group displayed lower p62 levels compared to MTX alone, suggesting that HBO therapy ameliorates MTX-induced autophagic dysregulation.

2.8.2 CA2 Region

In the CA2 region, a similar trend was observed (Fig. 5f–i, j). Positive p62 immunoreactivity, marked with black arrow, was most prominent in the MTX group, followed by the HBO, MTX + HBO, and SALINE groups ($p < 0.05$). The significantly lower expression in the MTX + HBO group compared with MTX highlights the regulatory effect of HBO

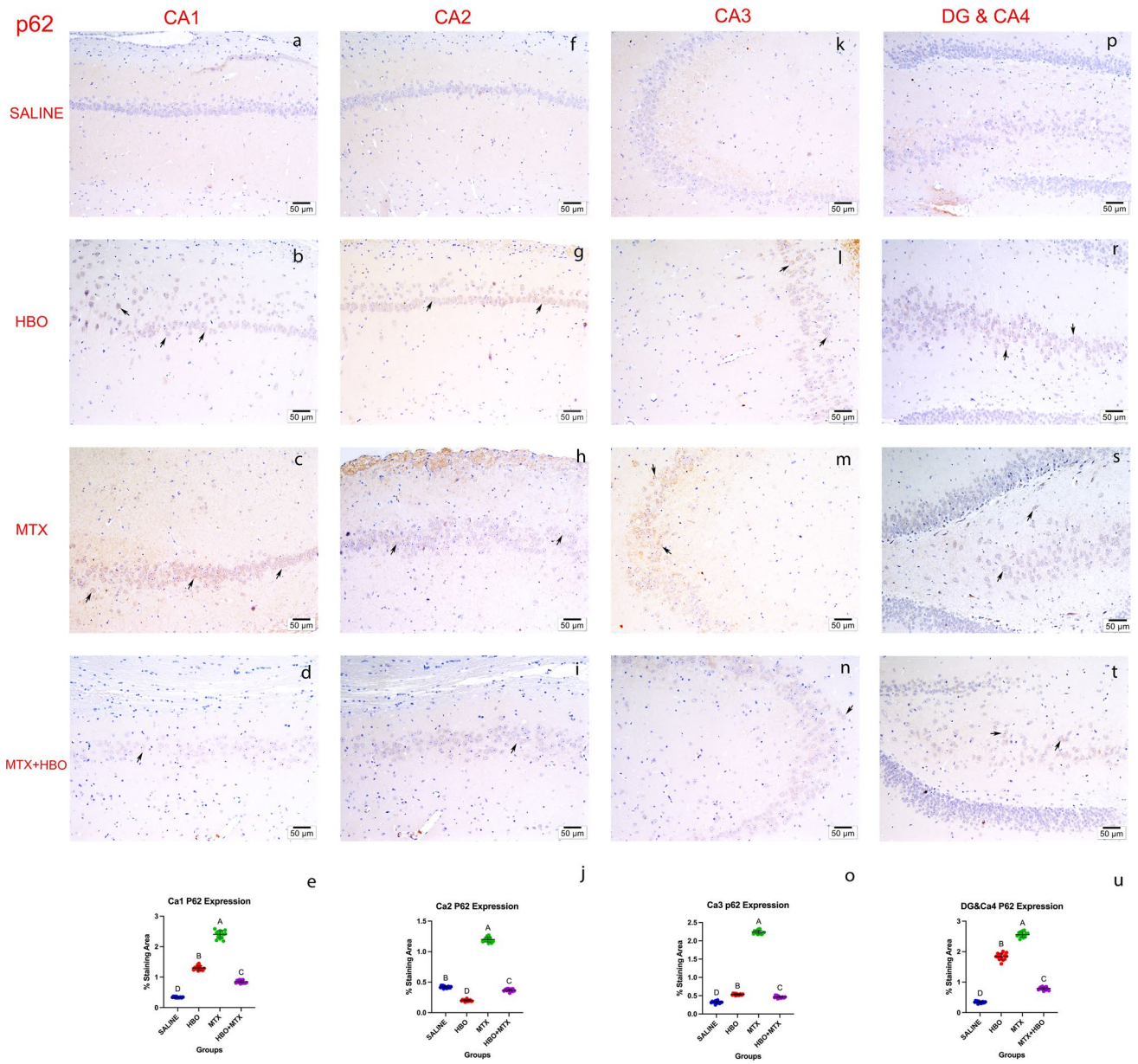

Fig. 5 Representative immunohistochemical images showing p62 expression in hippocampal subregions (CA1, CA2, CA3, DG&CA4) across experimental groups: SALINE (**a**, **f**, **k**, **p**), HBO (**b**, **g**, **l**, **r**), MTX (**c**, **h**, **m**, **s**), and MTX + HBO (**d**, **i**, **n**, **t**). Black arrow indicate p62-positive cells. Panels (e, j, o, u) represent quantitative analyses of p62 immunoreactivity expressed as % relative area in each subregion. Data are presented as dot plots showing individual animal values with mean ± SD. Serial sections were obtained from each animal, and two series were randomly selected per animal, with each series consisting of 12 sections. Quantification was performed using animal-based mean values, with each dot representing one animal (n = 7 per group).. Different superscript letters indicate statistically significant differences between groups ($p < 0.05$). Scale bars = 50 µm

on MTX-driven autophagy impairment. SALINE animals again exhibited the lowest baseline expression.

2.8.3 CA3 Region

P62 expression in the CA3 region of the hippocampus also varied significantly between groups (Fig. 5k–n, o). Black arrow indicate positive staining. The MTX group demonstrated the highest p62 expression ($p < 0.05$), reflecting methotrexate-induced autophagic accumulation. The HBO group showed moderate levels, while the MTX + HBO group exhibited a marked reduction compared to MTX alone. The SALINE group had minimal expression, consistent with physiological baseline levels. These findings indicate that HBO reduces MTX-mediated autophagic stress in the CA3 region.

2.8.4 DG & CA4 Regions

In the DG and CA4 regions, p62-positive cells were abundantly observed in the MTX group (Fig. 5p–t, u). Quantitative analysis revealed that the MTX group had the strongest expression ($p < 0.05$), followed by HBO, MTX + HBO, and SALINE groups. Expression in the MTX + HBO group was significantly lower than MTX, but higher than SALINE, confirming the attenuating effect of HBO therapy on MTX-induced autophagy impairment.

Statistical comparisons among groups were carried out by applying a one-way ANOVA, and multiple pairwise differences were assessed using the Tukey post-hoc procedure. In the bar graphs, groups annotated with distinct letters (A, B, C, D) were interpreted as being statistically different at a significance threshold of $p < 0.05$.

2.9 Beclin-1 Expression Findings

2.9.1 CA1 Region

Beclin-1 immunoreactivity in the CA1 region showed significant intergroup differences (Fig. 6a–d, e). Positively stained cells are indicated with black arrows. The MTX group demonstrated the highest Beclin-1 expression ($p < 0.05$), reflecting marked autophagic activation. The MTX + HBO group exhibited lower expression compared to MTX alone but remained higher than both HBO and SALINE groups. The SALINE group showed the lowest levels of expression, consistent with baseline physiological conditions.

2.9.2 CA2 Region

In the CA2 region, a similar distribution was observed (Fig. 6f–j). Black arrows indicate Beclin-1-positive cells. The MTX group again exhibited the highest Beclin-1 expression ($p < 0.05$), followed by MTX + HBO, HBO, and SALINEgroups. The reduction observed in the MTX + HBO group compared with MTX suggests that HBO co-treatment attenuates MTX-induced upregulation of Beclin-1.

2.9.3 CA3 Region

Beclin-1 immunoreactivity in the CA3 region also varied significantly among the groups (Fig. 6k–o). The MTX group displayed the strongest expression ($p < 0.05$), while the MTX + HBO group showed a reduced expression compared to MTX, though still elevated compared with SALINE and HBO groups. The HBO group showed moderate expression, and the SALINE group had the lowest levels. These findings suggest that MTX strongly induces Beclin-1 in CA3 neurons, while HBO treatment provides partial regulation.

2.9.4 DG & CA4 Regions

In the DG and CA4 regions, Beclin-1 immunopositive cells were most abundant in the MTX group**,** as highlighted by black arrows (Fig. 6p–u)**.** Quantitative analysis demonstrated that Beclin-1 expression in MTX-treated animals was significantly elevated compared to all other groups **($\mathbf{p} < 0.05$),** indicating a strong induction of autophagic signaling under methotrexate exposure. In contrast, the MTX + HBO group exhibited a noticeable reduction in Beclin-1 levels relative to MTX alone, although expression remained higher than in the SALINE and HBO groups. This suggests that HBO co-treatment partially counteracts the MTX-driven autophagic activation**.** The HBO group displayed a slight increase over the SALINE group, pointing to a potential stimulatory role of HBO itself on basal autophagy. Quantitative analysis revealed that the MTX group exhibited the highest expression levels ($p < 0.05$). In the MTX + HBO group, values were markedly reduced compared to MTX alone, though still above those observed in the SALINE group, indicating that HBO co-administration exerts a balancing influence on MTX-induced alterations. The HBO groupshowed a slight increase relative to SALINE.

Intergroup comparisons were conducted using a one-way ANOVA, and pairwise post-hoc analyses were carried out with the Tukey test. In the graphical representations, groups annotated with distinct letters (A, B, C, D) were considered significantly different at a threshold of $p < 0.05$.

This study is among the few investigations that comparatively examine the effects of low-dose MTX and HBO on the autophagy–apoptosis axis across different hippocampal subregions (CA1, CA2, CA3, DG & CA4). Our findings indicate that MTX initiates autophagy but fails to complete the flux, accompanied by increased pro-apoptotic activation (Caspase-3), whereas HBO partially restores this imbalance.

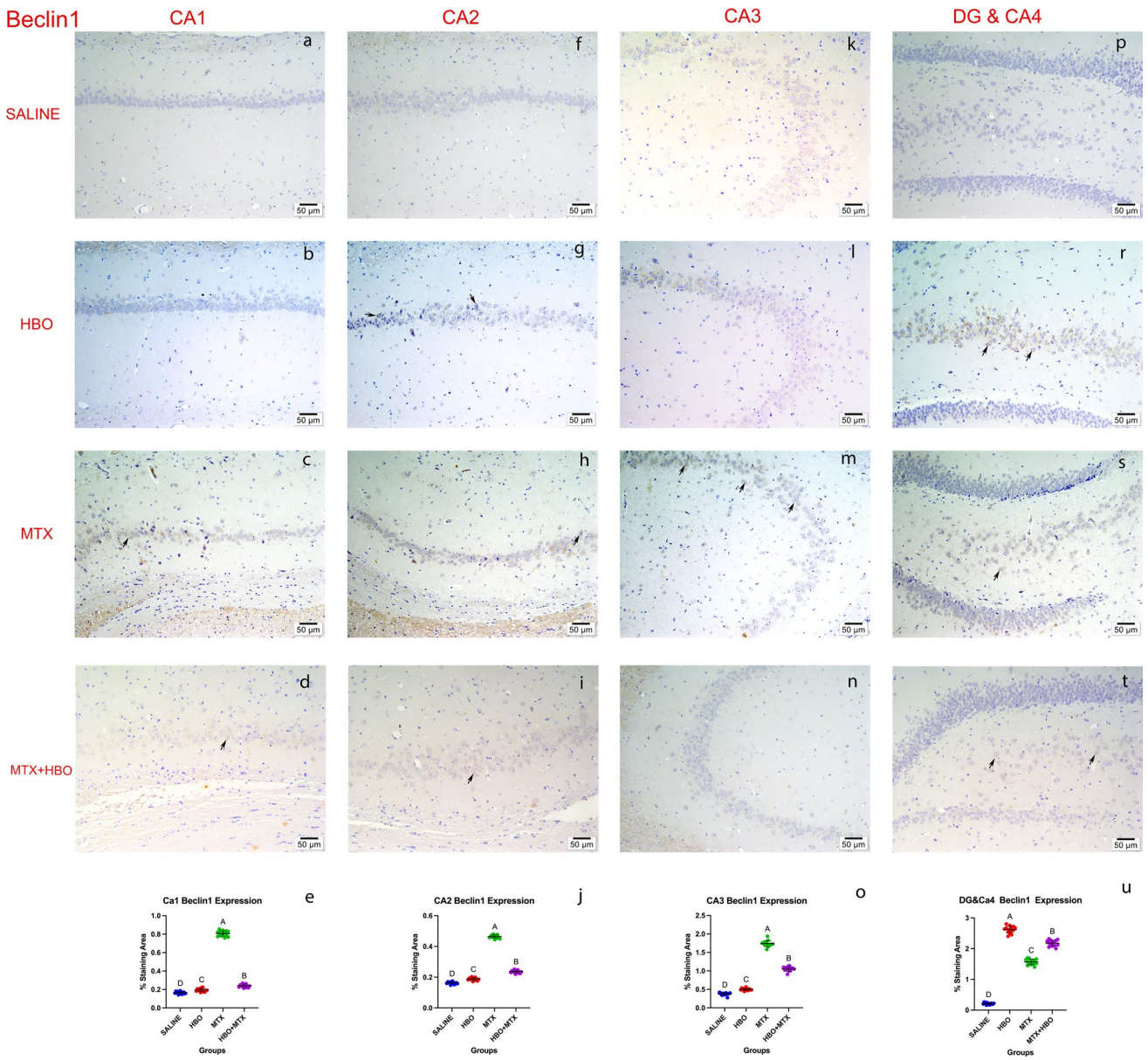

Fig. 6 Representative immunohistochemical images showing Beclin-1 expression in hippocampal subregions (CA1, CA2, CA3, DG&CA4) across experimental groups: SALINE (**a**, **f**, **k**, **p**), HBO (**b**, **g**, **l**, **r**), MTX (**c**, **h**, **m**, **s**), and MTX + HBO (**d**, **i**, **n**, **t**). Black arrows indicate Beclin-1-positive cells. Panels (e, j, o, u) represent quantitative analyses of Beclin-1 immunoreactivity expressed as % relative area in each subregion. Data are presented as dot plots showing individual animal values with mean ± SD. Serial sections were obtained from each animal, and two series were randomly selected per animal, with each series consisting of 12 sections. Quantification was performed using animal-based mean values, with each dot representing one animal (n = 7 per group). Different superscript letters indicate statistically significant differences between groups ($p < 0.05$). Scale bars = 50 µm

3 Discussion

Methotrexate was first introduced in the 1940s as a folic acid antagonist for the treatment of childhood leukemias and later became one of the standard agents in the management of both malignant and inflammatory diseases [1, 31]. The origins of hyperbaric oxygen therapy (HBO) date back to the seventeenth century; however, its scientific foundations were laid by Paul Bert, and from the mid-twentieth century onward, it entered modern clinical practice through the pioneering studies of Boerema and colleagues [31, 32]. Our results both overlap with and diverge from previous reports, and the underlying reasons for these discrepancies have been

evaluated in terms of methodological and pharmacodynamic differences.

3.1 Autophagy Initiation Signaling—Beclin-1 & LC3

LC3 was first identified in 1988 as a component of the microtubule-associated protein complex [33] and was later recognized as the mammalian homolog of yeast Atg8, subsequently being established as a fundamental marker of autophagy [34]. p62/SQSTM1 functions as a selective adaptor protein that links ubiquitinated cargo to LC3, thereby facilitating cargo sequestration into autophagosomes and serving as a critical interface between autophagy and cellular proteostasis [35]. Beclin-1 represents the first regulatory protein of autophagy identified in mammals and plays a pivotal role in autophagosome nucleation through its interaction with the class III PI3K complex [32, 34]. Initially described in human breast cancer cells, Beclin-1 was shown to function as a tumor suppressor and to be indispensable for the regulation of autophagic activity. In general, increased Beclin-1 expression is interpreted as activation of the autophagy initiation machinery and early autophagosomal membrane formation, whereas reduced levels are associated with suppression of autophagic activity [36, 37].

In the present study, MTX administration was associated with a statistically significant increase in both Beclin-1 and LC3 immunoreactivity within the pyramidal cell layers of the hippocampus (CA1–CA3), indicating activation of the autophagy initiation phase in these regions. In the MTX + HBO group, this initiation signal was largely preserved, whereas HBO alone induced a more limited elevation of Beclin-1 and LC3 in the same subfields. In contrast, within the DG&CA4 region, Beclin-1 immunoreactivity was more prominently enhanced following HBO exposure, suggesting that the neurogenic niche of the dentate gyrus may exhibit heightened sensitivity to oxygen-dependent modulation of the autophagy initiation complex. The regional pattern of LC3 expression, particularly within CA1–CA2, further supports the notion that early-phase autophagy initiation can be differentially regulated by MTX and HBO across distinct hippocampal subregions. Taken together, the autophagy-related changes observed under HBO treatment alone are best interpreted as an adaptive and non-pathological cellular response to increased oxygen availability, rather than as a pro-stress signal or overt autophagic activation.

This pattern of early-phase activation partially diverges from several MTX models reported in the literature. Sabry et al. [38] and Abd El-Aal et al. [39] described MTX-induced p62 accumulation and glial activation accompanied by reduced Beclin-1 and LC3 expression. While our findings are consistent with these studies in terms of downstream p62 accumulation and stress-related signaling, they additionally capture preserved or enhanced Beclin-1 and LC3 expression at the initiation stage. This apparent discrepancy may reflect differences in MTX dosage, exposure duration, and temporal sampling, with the present data likely representing an earlier phase characterized by robust initiation signaling preceding overt autophagic exhaustion. Importantly, the observed increases in Beclin-1 and LC3 should not be interpreted as evidence of fully functional autophagy; rather, when considered together with p62 accumulation and Caspase-3 activation, they suggest a state in which autophagy is initiated but may not proceed efficiently. Collectively, these findings underscore that early-phase markers alone do not necessarily reflect effective autophagic flux, but instead provide insight into region-specific activation patterns within a complex and potentially dysregulated autophagy–apoptosis landscape.

3.2 Autophagic Flux Status—p62/SQSTM1

p62/SQSTM1 functions as an adaptor protein that links ubiquitinated proteins to LC3, thereby serving as a cargo receptor in the autophagic process [35]. Owing to this role, p62 has been widely used as an indicator of autophagic flux. In general, p62 accumulation is observed when autophagosome clearance or lysosomal degradation is impaired [40, 41], whereas reduced p62 levels are commonly associated with ongoing cargo degradation and progression of the autophagic process [35]. However, it should be noted that p62 abundance is not exclusively regulated by autophagy, as it is also subject to transcriptional control, particularly via the NRF2 pathway, and may be influenced by proteasomal activity.

In the present study, MTX administration was associated with a marked increase in p62 immunoreactivity across hippocampal subregions. This elevation, occurring concomitantly with preserved or enhanced Beclin-1 and LC3 expression, is consistent with a scenario in which autophagy is initiated but may not efficiently progress through later degradative stages. In the MTX + HBO group, p62 immunoreactivity was significantly reduced compared with MTX alone, and in certain subregions, HBO treatment alone was associated with lower basal p62 levels. Rather than providing definitive proof of restored autophagic flux, this pattern suggests that HBO may exert a modulatory influence on downstream autophagy-related pathways that favor more effective cargo handling under MTX-induced stress conditions.

Our findings are broadly consistent with previous MTX models reported by Sabry et al. (2024) and Abd El-Aal et al. (2024), both of which demonstrated pronounced p62 accumulation following MTX exposure [38, 39]. In those studies, p62 elevation was interpreted as evidence of autophagic flux disruption, and Abd El-Aal et al. further showed that p62 accumulation could be attenuated by antioxidant-based

interventions. In line with these observations, the reduction of p62 immunoreactivity observed in the MTX + HBO group in the present study suggests that improved cellular redox or metabolic conditions may partially alleviate MTX-associated autophagy dysregulation. Nevertheless, given the multifactorial regulation of p62, these findings should be interpreted cautiously and not as conclusive evidence of fully restored autophagic flux.

Taken together, the p62/SQSTM1 expression profile supports a model in which MTX exposure is associated with preserved autophagy initiation signals but compromised downstream processing, whereas HBO treatment appears to mitigate, rather than completely reverse, this imbalance. When considered alongside the concomitant increase in Caspase-3 under MTX and its attenuation in the MTX + HBO group, the data indicate that HBO modulates the autophagy–apoptosis axis in a manner that may reduce cellular stress and apoptotic signaling, without allowing definitive conclusions regarding complete functional recovery of autophagic flux.

3.2.1 Apoptotic Signaling— Cleaved Caspase-3 (Asp175)

Caspase-3 is the most extensively characterized executioner protease of the apoptotic cascade. Initially identified in the early 1990s under different names, including CPP32, apopain, and Yama, these proteins were subsequently recognized as a single enzyme formally designated as Caspase-3. Nicholson et al. (1995) demonstrated that Caspase-3 is indispensable for programmed cell death in mammals, thereby establishing its central role in apoptotic signaling [42]. Caspase-3 contributes to the morphological and biochemical features of apoptosis through the cleavage of multiple downstream substrates, including PARP, ICAD, and fodrin, which are involved in chromatin condensation, cytoskeletal reorganization, and DNA fragmentation [42, 43]. Accordingly, increased Caspase-3 immunoreactivity is widely interpreted as activation of apoptotic signaling pathways, whereas reduced expression is generally associated with attenuation of apoptotic processes and enhanced cellular survival [44, 45].

In the present study, MTX administration was associated with a statistically significant increase in Caspase-3 immunoreactivity across all examined hippocampal subregions (CA1, CA2, CA3, and DG/CA4). This elevation occurred in parallel with preserved or enhanced autophagy initiation signals, as indicated by Beclin-1 and LC3 expression, and coincided with p62 accumulation, suggesting that cellular stress responses may have shifted toward apoptotic signaling when downstream autophagic processing was compromised. HBO treatment alone resulted in Caspase-3 levels that were modestly elevated relative to control in selected regions but markedly lower than those observed under MTX exposure. Notably, combined MTX + HBO treatment significantly reduced Caspase-3 immunoreactivity compared with MTX alone, indicating attenuation of pro-apoptotic signaling rather than complete suppression of apoptotic pathways.

These findings are consistent with previous reports demonstrating MTX-induced Caspase-3 activation and concomitant apoptotic vulnerability in neural tissue. Sabry et al. (2024) reported increased Caspase-3 expression following MTX exposure, while other studies have shown that autophagy dysregulation under MTX conditions is frequently accompanied by enhanced apoptotic signaling [38]. Extending these observations, our region-specific analysis suggests that pyramidal fields (CA1–CA3) exhibit more pronounced Caspase-3 activation, whereas in the DG&CA4 region, HBO treatment was associated with enhanced autophagy initiation signals alongside reduced Caspase-3 expression. This pattern supports the notion that HBO modulates the balance between autophagy-related stress responses and apoptotic signaling in a region-dependent manner, rather than directly restoring fully functional autophagy.

Despite the observed increase in Caspase-3 immunoreactivity, the absence of TUNEL positivity indicates that apoptotic progression may have been captured at an early or pre-fragmentation stage. DNA fragmentation represents a relatively late event in apoptosis and depends on activation of the ICAD/CAD axis, whereby caspase-mediated cleavage of ICAD releases CAD to induce internucleosomal DNA breaks [43, 46–48]. Because the TUNEL assay specifically labels exposed 3′-OH DNA ends [49], its negativity does not exclude the presence of early apoptotic signaling. Apoptosis may remain below the threshold required for detectable DNA fragmentation, or technical factors such as tissue fixation and limited TdT accessibility may reduce assay sensitivity. In addition, both false-negative and false-positive TUNEL results have been reported under specific experimental conditions [50]. Within this context, the reduction of Caspase-3 immunoreactivity observed in the MTX + HBO group may have further contributed to TUNEL negativity, emphasizing that TUNEL findings should be interpreted in conjunction with upstream apoptotic markers, such as cleaved Caspase-3, PARP cleavage, or ICAD/CAD signaling, rather than as standalone evidence of apoptotic absence (Tables 2, 3, 4, 5, 6).

4 Conclusions

In the rat hippocampus, low-dose methotrexate (MTX) is associated with activation of the autophagy initiation machinery, as reflected by increased Beclin-1 and LC3 immunoreactivity. However, this response appears to be accompanied by p62/SQSTM1 accumulation and elevated Cleaved Caspase-3 (Asp175) immunoreactivity, a pattern

Table 2 Semi-quantitative evaluation of LC3 immunoreactivity in hippocampal subregions (CA1, CA2, CA3, DG&CA4) across experimental groups (SALINE, HBO, MTX, MTX + HBO)

LC3	CA1	CA2	CA3	DG & CA4
Sham	n: –	n: –	n: –	n: –
	c: +	c: +	c: +	c: +
	np: +	np: ++	np: ++	np: +++
HBO	n: –	n: –	n: –	n: –
	c: ++	c: ++	c: +	c: ++
	np: +	np: +	np: +	np: +++
MTX	n: –	n: –	n: –	n: –
	c: +++	c: +++	c: +++	c: +++
	np: +	np: +++	np: +++	np: +++
MTX + HBO	n: –	n: –	n: –	n: –
	c: +++	c: +++	c: +++	c: +++
	np: +	np: +	np: ++	np: +++

Localization of staining is indicated for nucleus (n), cytoplasm (c), and neuropil (np). Staining intensity is graded as negative (−), weak (+), moderate (++), and strong (+++)

Nucleus: n

Cytoplasm: c

Neuropil: np

Table 3 Semi-quantitative evaluation of Cleaved Caspase-3 (Asp175) immunoreactivity in hippocampal subregions (CA1, CA2, CA3, DG&CA4) across experimental groups (SALINE, HBO, MTX, MTX + HBO)

Caspase 3	CA1	CA2	CA3	DG & CA4
Sham	n: +	n: +	n: +	n: +
	c: –	c: –	c: –	c: –
	np: –	np: –	np: –	np: –
HBO	n: ++	n: ++	n: +	n: +
	c: –	c: –	c: –	c: –
	np: –	np: –	np: –	np: –
MTX	n: +++	n: +++	n: +++	n: +++
	c: –	c: –	c: –	c: –
	np: –	np: –	np: –	np: –
MTX + HBO	n: ++	n: ++	n: ++	n: +
	c: –	c: –	c: –	c: –
	np: –	np: –	np: –	np: –

Localization of staining is indicated for nucleus (n), cytoplasm (c), and neuropil (np). Staining intensity is graded as negative (−), weak (+), moderate (++), and strong (+++)

Nucleus: n

Cytoplasm: c

Neuropil: np

Table 4 Semi-quantitative evaluation of p62 immunoreactivity in hippocampal subregions (CA1, CA2, CA3, DG&CA4) across experimental groups (SALINE, HBO, MTX, MTX + HBO)

p62	CA1	CA2	CA3	DG & CA4
Sham	n: –	n: –	n: –	n: –
	c: – / +	c: – / +	c: – / +	c: +
	np: – / +	np: – / +	np: – / +	np: ++
HBO	n: –	n: –	n: –	n: –
	c: +	c: +	c: +	c: +
	np: ++	np: +	np: +	np: ++
MTX	n: –	n: –	n: –	n: –
	c: ++	c: ++	c: ++	c: ++
	np: +	np: +	np: ++	np: ++
MTX + HBO	n: –	n: –	n: –	n: –
	c: +	c: +	c: +	c: +
	np: +	np: +	np: +	np: ++

Localization of staining is indicated for nucleus (n), cytoplasm (c), and neuropil (np). Staining intensity is graded as negative (−), weak (+), moderate (++), and strong (+++)

Nucleus: n

Cytoplasm: c

Neuropil: np

Table 5 Semi-quantitative evaluation of Beclin-1 immunoreactivity in hippocampal subregions (CA1, CA2, CA3, DG&CA4) across experimental groups (SALINE, HBO, MTX, MTX + HBO)

Beclin1	CA1	CA2	CA3	DG & CA4
Sham	n: –	n: –	n: –	n: –
	c: – / +	c: – / +	c: +	c: – / +
	np: – / +	np: +	np: +	np: +
HBO	n: –	n: –	n: –	n: –
	c: +	c: +	c: +	c: ++
	np: +	np: +	np: +	np: ++
MTX	n: –	n: –	n: –	n: –
	c: ++	c: ++	c: +++	c: +++
	np: +	np: +	np: ++	np: ++
MTX + HBO	n: –	n: –	n: –	n: –
	c: +	c: ++	c: +	c: +
	np: +	np: +	np: +	np: +

Localization of staining is indicated for nucleus (n), cytoplasm (c), and neuropil (np). Staining intensity is graded as negative (−), weak (+), moderate (++), and strong (+++)

Nucleus: n

Cytoplasm: c

Neuropil: np

that is consistent with incomplete downstream autophagic processing and enhanced apoptotic signaling rather than fully functional autophagy. Hyperbaric oxygen (HBO) treatment modifies this response profile: while early-phase autophagy markers remain preserved, p62 and Caspase-3 levels are reduced relative to MTX alone, suggesting a partial attenuation of autophagy-related stress and pro-apoptotic signaling rather than definitive restoration of autophagic flux.

These effects display clear regional specificity within the hippocampus. MTX-related alterations are most prominent in the pyramidal fields (CA1–CA3), whereas HBO is associated with a more pronounced Beclin-1 response in the

Table 6 Semi-quantitative evaluation of TUNEL staining in hippocampal subregions (CA1, CA2, CA3, DG&CA4) across experimental groups (SALINE, HBO, MTX, MTX + HBO)

Tunel	CA1	CA2	CA3	DG & CA4
Sham	n: –	n: –	n: –	n: –
	c: –	c: –	c: –	c: –
	np: –	np: –	np: –	np: –
HBO	n: –	n: –	n: –	n: –
	c: –	c: –	c: +	c: –
	np: –	np: –	np: –	np: –
MTX	n: –	n: –	n: –	n: –
	c: –	c: –	c: –	c: –
	np: –	np: –	np: –	np: –
MTX + HBO	n: –	n: –	n: –	n: –
	c: –	c: –	c: –	c: –
	np: –	np: –	np: –	np: –

Localization of staining is indicated for nucleus (n), cytoplasm (c), and neuropil (np). All groups showed negative TUNEL staining (−) in examined regions

Nucleus: n

Cytoplasm: c

Neuropil: np

DG&CA4 region, highlighting the differential sensitivity of hippocampal microenvironments to metabolic and oxygen-dependent modulation. Importantly, the absence of TUNEL positivity despite increased Caspase-3 immunoreactivity indicates that apoptotic processes were likely captured at an early or pre-fragmentation stage and/or that methodological factors related to tissue fixation and processing limited TUNEL sensitivity. This finding underscores the necessity of interpreting TUNEL results in conjunction with upstream apoptotic markers when assessing neuronal vulnerability.

Collectively, the present data support a conceptual framework in which MTX exposure promotes a state characterized by preserved autophagy initiation but compromised downstream processing, coinciding with increased apoptotic signaling. Within this context, HBO appears to shift the balance toward a less pro-apoptotic cellular milieu, potentially through modulation of autophagy-associated stress pathways. While these findings identify HBO as a biologically plausible modulatory intervention in MTX-associated hippocampal stress, definitive conclusions regarding restored autophagic flux or long-term neuroprotection cannot be drawn from the present data alone. Accordingly, future studies incorporating time-resolved analyses, direct assessments of autophagic flux and lysosomal competence, and functional or behavioral outcomes will be essential to further define the therapeutic relevance of the autophagy–apoptosis axis in MTX-induced neurotoxicity.

5 Limitations

Several limitations of the present study should be acknowledged. First, the experiments were conducted exclusively in male rats; therefore, potential sex-specific differences in autophagy and apoptotic signaling, which may be influenced by estrogen-dependent modulation of mitochondrial function and oxidative stress responses, were not addressed. Second, although methotrexate is well known to disrupt folate metabolism and induce functional folate deficiency, folic acid levels were not directly measured in the present study; instead, folate deficiency was inferred based on the established pharmacological mechanism of MTX and consistent evidence from previous experimental and clinical studies. Third, although autophagy-related markers were comprehensively analyzed, autophagic flux was not directly assessed using lysosomal markers or pharmacological flux assays; accordingly, conclusions regarding flux completion should be interpreted cautiously. Fourth, the absence of behavioral or cognitive assessments limits the direct functional interpretation of the observed histological and molecular changes. Finally, despite increased Caspase-3 immunoreactivity, the lack of TUNEL positivity suggests that apoptotic processes were captured at an early stage and/or that methodological factors related to tissue fixation and assay sensitivity may have influenced detection. These limitations highlight the need for future studies incorporating both sexes, direct flux measurements, biochemical confirmation of folate status, and functional readouts to further define the autophagy–apoptosis axis in MTX-induced neurotoxicity.

Acknowledgements The authors would like to thank the staff of the Erciyes University Scientific Research Projects (BAP) Unit for their administrative and technical support. This study was financially supported by Erciyes University Scientific Research Projects (BAP) Unit under project code TSA-2023-13404

Authors Contribution A.C.: Performed the immunohistochemical staining, conducted the statistical analysis, prepared the figures, and wrote the manuscript. M.A.B.: Applied the hyperbaric oxygen therapy and critically reviewed the manuscript. B.K.: Actively assisted in the experimental procedures. M.E.: Coordinated, organized, and supervised the experimental procedures. E.C.: Actively assisted in the experimental procedures. F.B.: Managed the experimental processes and performed a detailed critical review of the manuscript.

Funding Open access funding provided by the Scientific and Technological Research Council of Türkiye (TÜBİTAK). This study was financially supported by Erciyes University Scientific Research Projects (BAP) Unit under project code TSA-2023–13404.

Data Availability All data generated or analyzed during this study are available from the authors on reasonable request.

Declarations

Conflict of interest The authors declare no competing interests.

Ethical Approval All animal-related procedures were reviewed and approved by the Local Ethics Committee for Animal Experiments at Erciyes University (Approval No: 22/120, Kayseri, Turkey) and were carried out in accordance with both institutional policies and international standards for ethical animal research.

Open Access This article is licensed under a Creative Commons Attribution 4.0 International License, which permits use, sharing, adaptation, distribution and reproduction in any medium or format, as long as you give appropriate credit to the original author(s) and the source, provide a link to the Creative Commons licence, and indicate if changes were made. The images or other third party material in this article are included in the article's Creative Commons licence, unless indicated otherwise in a credit line to the material. If material is not included in the article's Creative Commons licence and your intended use is not permitted by statutory regulation or exceeds the permitted use, you will need to obtain permission directly from the copyright holder. To view a copy of this licence, visit http://creativecommons.org/licenses/by/4.0/.

References

1. Farber S, Dıamond L. Temporary remissions in acute leukemia in children produced by folic acid antagonist, 4-aminopteroylglutamic acid. N Engl J Med. 1948;238(23):787–93. https://doi.org/10.1056/NEJM194806032382301.
2. Hanoodi M, Mittal M. Methotrexate. In: StatPearls. Treasure Island (FL): StatPearls Publishing; December 11, 2024.
3. Han P, Liu X, He J, Han L, Li J. Overview of mechanisms and novel therapies on rheumatoid arthritis from a cellular perspective. Front Immunol. 2024;15:1461756. https://doi.org/10.3389/fimmu.2024.1461756.
4. Mocanu M, Procopciuc D, Gheucă-Solovăstru DF, et al. An overview of methotrexate indications in skin diseases. Medicina Kaunas. 2024;60(7):1024. https://doi.org/10.3390/medicina60071024.
5. Kadry MO, Ammar NM, Hassan HA, Abdel Megeed RM. Insights on attenuating autophagy cellular and molecular pathways versus methotrexate-induced toxicity via liposomal turmeric therapy. J Genet Eng Biotechnol. 2022;20(1):147. https://doi.org/10.1186/s43141-022-00430-4.
6. Wasfey EF, Shaaban M, Essam M, et al. Infliximab ameliorates methotrexate-induced nephrotoxicity in experimental rat model: impact on oxidative stress, mitochondrial biogenesis, apoptotic and autophagic machineries. Cell Biochem Biophys. 2023;81(4):717–26. https://doi.org/10.1007/s12013-023-01168-7.
7. Thom SR. Hyperbaric oxygen: its mechanisms and efficacy. Plast Reconstr Surg. 2011;127(Supp1):131S-141S. https://doi.org/10.1097/PRS.0b013e3181fbe2bf.
8. Huang ET, editor. Hyperbaric medicine indications manual. 15th ed. North Palm Beach, FL: Best Publishing Company; 2023.
9. Heyboer M, Sharma D, Santiago W, McCulloch N. Hyperbaric oxygen therapy: side effects defined and quantified. Adv Wound Care. 2017;6(6):210–24. https://doi.org/10.1089/wound.2016.0718.
10. Buras J. Basic mechanisms of hyperbaric oxygen in the treatment of ischemia-reperfusion injury. Int Anesthesiol Clin. 2000;38(1):91–109. https://doi.org/10.1097/00004311-200001000-00007.
11. Ostrowski RP, Colohan AR, Zhang JH. Neuroprotective effect of hyperbaric oxygen in a rat model of subarachnoid hemorrhage. Acta Neurochir Suppl. 2006;96:188–93. https://doi.org/10.1007/3-211-30714-1_41.
12. Chen W, Lv L, Nong Z, Chen X, Pan X, Chen C. Hyperbaric oxygen protects against myocardial ischemia-reperfusion injury through inhibiting mitochondria dysfunction and autophagy. Mol Med Rep. 2020;22(5):4254–64. https://doi.org/10.3892/mmr.2020.11497.
13. Wang C, Niu F, Ren N, et al. Hyperbaric oxygen improves cerebral ischemia/reperfusion injury in rats probably via inhibition of autophagy triggered by the downregulation of hypoxia-inducing factor-1 alpha. BioMed Res Int. 2021;2021(1):6615685. https://doi.org/10.1155/2021/6615685.
14. Mizushima N, Komatsu M. Autophagy: renovation of cells and tissues. Cell. 2011;147(4):728–41. https://doi.org/10.1016/j.cell.2011.10.026.
15. Pedrycz A, Kozakiewicz M, Rahnama M, et al. Hyperbaric treatment stimulates chaperone-mediated macroautophagy and autophagy in the liver cells of healthy female rats. Int J Mol Sci. 2024;25(19):10476. https://doi.org/10.3390/ijms251910476.
16. Bartsch T, Wulff P. The hippocampus in aging and disease: from plasticity to vulnerability. Neuroscience. 2015;309:1–16. https://doi.org/10.1016/j.neuroscience.2015.07.084.
17. Jones MW, McHugh TJ. Updating hippocampal representations: CA2 joins the circuit. Trends Neurosci. 2011;34(10):526–35. https://doi.org/10.1016/j.tins.2011.07.007.
18. Kesner RP. A process analysis of the CA3 subregion of the hippocampus. Front Cell Neurosci. 2013;7:78. https://doi.org/10.3389/fncel.2013.00078.
19. Scharfman HE. The CA3 "backprojection" to the dentate gyrus. Prog Brain Res. 2007;163:627–37. https://doi.org/10.1016/S0079-6123(07)63034-9.
20. Beyaz F. Structural and functional properties of hippocampal neurons. In: Turgut M, Acer N, Turgut AT, Di Rocco C, eds. The human hippocampus. Springer; 2025. https://doi.org/10.1007/978-3-031-88907-3_4.
21. Christian KM, Song H, Ming GL. Functions and dysfunctions of adult hippocampal neurogenesis. Annu Rev Neurosci. 2014;37:243–62. https://doi.org/10.1146/annurev-neuro-071013-014134.
22. El-Falougy H, Benuska J. History, anatomical nomenclature, comparative anatomy and functions of the hippocampal formation. Bratisl Lek Listy. 2006;107(4):103–6.
23. Baktir MA, Suer C, Dolu N, Artis AS. In vivo investigation of the effects of light/dark cycle changes on synaptic plasticity in the dentate gyrus of the rat hippocampus. Exp Biomed Res. 2025;8(3):188–202. https://doi.org/10.30714/j-ebr.2025.248.
24. Yin B, Barrionuevo G, Batinic-Haberle I, Sandberg M, Weber SG. Differences in reperfusion-induced mitochondrial oxidative stress and cell death between hippocampal CA1 and CA3 subfields are due to the mitochondrial thioredoxin system. Antioxid Redox Signal. 2017;27(9):534–49. https://doi.org/10.1089/ars.2016.6706.
25. Li J, Ning Z, Zhong X, et al. Dynamic changes in Beclin-1, LC3B, and p62 in aldose reductase-knockout mice at different time points after ischemic stroke. Heliyon. 2024;10(19):e38068. https://doi.org/10.1016/j.heliyon.2024.e38068.
26. Liu K, Yao X, Gao J, Wang J, Qi J. A study on the mechanism of Beclin-1 m6A modification mediated by catalpol in protection against neuronal injury and autophagy following cerebral ischemia. Mol Med. 2024;30(1):65. https://doi.org/10.1186/s10020-024-00818-7.
27. Baktir MA, Calik O, Basaran KE, Turker BG, Suer C. Hyperbaric oxygen therapy enhances hippocampal long-term potentiation via upregulation of BDNF and p-CREB1 in rats: evidence outside pathological models. Neuroscience. 2025;584:279–85. https://doi.org/10.1016/j.neuroscience.2025.08.045.
28. Van Pelt LF. Ketamine and xylazine for surgical anesthesia in rats. J Am Vet Med Assoc. 1977;171(9):842–4.
29. Özbek M, Cabir A, Beyaz F, Karaca H, Öztop M. Differential expression of VGLUT1, GAD65, GAD67, and MAP2 in the retina of hibernating Anatolian ground squirrel (*Spermophilus*

xanthoprymnus). Ann Anat. 2025;263:152729. https://doi.org/10.1016/j.aanat.2025.152729.
30. Özbek M, Beyaz F, Öztop M, Karaca H, Cabir A, Kiryar BF. Anatolian ground squirrel (*Spermophilus xanthoprymnus*) retina: comparative expression of synaptophysin, NeuN, calbindin-D28k, parvalbumin, glial fibrillary acidic protein, and Iba-1 during prehibernation and hibernation. Anat Rec. 2025. https://doi.org/10.1002/ar.25682.
31. Weinblatt ME, Coblyn JS, Fox DA, et al. Efficacy of low-dose methotrexate in rheumatoid arthritis. N Engl J Med. 1985;312(13):818–22. https://doi.org/10.1056/NEJM198503283121303.
32. Boerema I, Meyne Ng, Brummelkamp Wh, et al. Ned Tijdschr Geneeskd. 1960;104:949–954.
33. Mann SS, Hammarback JA. Molecular characterization of light chain 3. A microtubule binding subunit of MAP1A and MAP1B. J Biol Chem. 1994;269(15):11492–7.
34. Kabeya Y, Mizushima N, Ueno T. LC3, a mammalian homologue of yeast Apg8p, is localized in autophagosome membranes after processing. EMBO J. 2000;19(21):5720–8. https://doi.org/10.1093/emboj/19.21.5720.
35. Bjørkøy G, Lamark T, Brech A, et al. p62/SQSTM1 forms protein aggregates degraded by autophagy and has a protective effect on huntingtin-induced cell death. J Cell Biol. 2005;171(4):603–14. https://doi.org/10.1083/jcb.200507002.
36. Liang F, Han M, Romanienko PJ, Jasin M. Homology-directed repair is a major double-strand break repair pathway in mammalian cells. Proc Natl Acad Sci U S A. 1998;95(9):5172–7. https://doi.org/10.1073/pnas.95.9.5172.
37. Pattingre S, Tassa A, Qu X, et al. Bcl-2 antiapoptotic proteins inhibit Beclin 1-dependent autophagy. Cell. 2005;122(6):927–39. https://doi.org/10.1016/j.cell.2005.07.002.
38. Sabry NC, Michel HE, Menze ET. Repurposing of erythropoietin as a neuroprotective agent against methotrexate-induced neurotoxicity in rats. J Psychopharmacol. 2025;39(2):147–63. https://doi.org/10.1177/02698811241295379.
39. Abd El-Aal SA, El-Sayyad SM, El-Gazar AA, et al. Boswellic acid and apigenin alleviate methotrexate-provoked renal and hippocampal alterations in rats: targeting autophagy, NOD-2/NF-κB/NLRP3, and connexin-43. Int Immunopharmacol. 2024;134:112147. https://doi.org/10.1016/j.intimp.2024.112147.
40. Komatsu M, Waguri S, Koike M, et al. Homeostatic levels of p62 control cytoplasmic inclusion body formation in autophagy-deficient mice. Cell. 2007;131(6):1149–63. https://doi.org/10.1016/j.cell.2007.10.035.
41. Mathew R, Karp CM, Beaudoin B, et al. Autophagy suppresses tumorigenesis through elimination of p62. Cell. 2009;137(6):1062–75. https://doi.org/10.1016/j.cell.2009.03.048.
42. Nicholson DW, Ali A, Thornberry NA, et al. Identification and inhibition of the ICE/CED-3 protease necessary for mammalian apoptosis. Nature. 1995;376(6535):37–43. https://doi.org/10.1038/376037a0.
43. Porter AG, Jänicke RU. Emerging roles of caspase-3 in apoptosis. Cell Death Differ. 1999;6(2):99–104. https://doi.org/10.1038/sj.cdd.4400476.
44. Devarajan E, Sahin AA, Chen JS, et al. Down-regulation of caspase 3 in breast cancer: a possible mechanism for chemoresistance. Oncogene. 2002;21(57):8843–51. https://doi.org/10.1038/sj.onc.1206044.
45. Chen J, Li HM, Zhang XN, Xiong CM, Ruan JL. Dioscin-induced apoptosis of human LNCaP prostate carcinoma cells through activation of caspase-3 and modulation of Bcl-2 protein family. J Huazhong Univ Sci Technol Med Sci. 2014;34(1):125–30. https://doi.org/10.1007/s11596-014-1243-y.
46. Enari M, Sakahira H, Yokoyama H, Okawa K, Iwamatsu A, Nagata S. A caspase-activated DNase that degrades DNA during apoptosis, and its inhibitor ICAD. Nature. 1998;391(6662):43–50. https://doi.org/10.1038/34112.
47. Sakahira H, Enari M, Nagata S. Cleavage of CAD inhibitor in CAD activation and DNA degradation during apoptosis. Nature. 1998;391(6662):96–9. https://doi.org/10.1038/34214.
48. Jänicke RU, Ng P, Sprengart ML, Porter AG. Caspase-3 is required for alpha-fodrin cleavage but dispensable for cleavage of other death substrates in apoptosis. J Biol Chem. 1998;273(25):15540–5. https://doi.org/10.1074/jbc.273.25.15540.
49. Gavrieli Y, Sherman Y, Ben-Sasson SA. Identification of programmed cell death in situ via specific labeling of nuclear DNA fragmentation. J Cell Biol. 1992;119(3):493–501. https://doi.org/10.1083/jcb.119.3.493.
50. Grasl-Kraupp B, Ruttkay-Nedecky B, Koudelka H, Bukowska K, Bursch W, Schulte-Hermann R. In situ detection of fragmented DNA (TUNEL assay) fails to discriminate among apoptosis, necrosis, and autolytic cell death: a cautionary note. Hepatology. 1995;21(5):1465–8. https://doi.org/10.1002/hep.1840210534.

Publisher's Note Springer Nature remains neutral with regard to jurisdictional claims in published maps and institutional affiliations.

Authors and Affiliations

A. Cabir[1] · M. A. Baktır[2] · B. F. Kıryar[3] · M. Ermiş[4] · E. Çolak[1] · F. Beyaz[1,3]

✉ A. Cabir
ahmetcabirvet@gmail.com; ahmetcabir@erciyes.edu.tr

M. A. Baktır
mabaktir@erciyes.edu.tr

B. F. Kıryar
begumkiryar@hotmail.com

M. Ermiş
mermis@erciyes.edu.tr

E. Çolak
colakk.emell@gmail.com

F. Beyaz
fbeyaz@erciyes.edu.tr

[1] Department of Histology and Embryology, Faculty of Veterinary Medicine, Erciyes University, Kayseri, Turkey

[2] Department of Physiology, Faculty of Medicine, Erciyes University, Kayseri, Turkey

[3] Department of Neuroscience, Gevher Nesibe Genome and Stem Cell Center, Erciyes University, Kayseri, Turkey

[4] Experimental Research Application and Research Center, Erciyes University, Kayseri, Turkey